Experimental Characterization of Quantum Dynamics Through Many-Body Interactions

Daniel Nigg, Julio T. Barreiro, Philipp Schindler, Masoud Mohseni, Thomas Monz, Michael Chwalla, Markus Hennrich, and Rainer Blatt

Phys. Rev. Lett. **110**, 060403 — Published 5 February 2013

DOI: 10.1103/PhysRevLett.110.060403

Experimental characterization of quantum dynamics through many-body interactions

Daniel Nigg[1], Julio T. Barreiro[1],* Philipp Schindler[1], Masoud Mohseni[3],†
Thomas Monz[1], Michael Chwalla[1,2], Markus Hennrich[1], and Rainer Blatt[1,2]
[1]*Institut für Experimentalphysik, Universität Innsbruck, Technikerstrasse 25, A–6020 Innsbruck, Austria*
[2]*Institut für Quantenoptik und Quanteninformation der Österreichischen Akademie der Wissenschaften, Technikerstrasse 21a, A–6020 Innsbruck, Austria*
[3]*Research Laboratory of Electronics, Massachusetts Institute of Technology, Massachusetts 02139, USA*

We report on the implementation of a quantum process tomography (QPT) technique known as direct characterization of quantum dynamics (DCQD) applied on coherent and incoherent single-qubit processes in a system of trapped $^{40}Ca^{+}$ ions. Using quantum correlations with an ancilla qubit, DCQD reduces substantially the number of experimental configurations required for a full QPT and all diagonal elements of the process matrix can be estimated with a single setting. With this technique, the system's relaxation times T_1 and T_2 were measured with a single experimental configuration. We further show the first, complete characterization of single-qubit processes using a single generalized measurement realized through multi-body correlations with three ancilla qubits.

PACS numbers: 03.67.Ac; 03.65.Wj

Characterization of quantum dynamics is an important primitive in quantum physics, chemistry, and quantum information science for determining unknown environmental interactions, estimating Hamiltonian parameters, and verifying the performance of engineered quantum devices. This has led to a major effort in developing tools for the full characterization of quantum processes, known as quantum process tomography (QPT). The standard approach for QPT is resource intensive, requiring 12^N experimental configurations for a system of N qubits [1, 2], where each experimental configuration consists of the preparation of input probe states and the measurement of process outputs [3]. Using ancilla qubits but only joint separable measurements, the number of experimental configurations is still 12^N [4–6]. However, the use of many-body interactions to ancilla qubits in the preparation and/or measurements can significantly decrease this number to anywhere from 4^N to a single configuration depending on the nature and complexity of quantum correlations [6]. Using two-body correlations DCQD requires up to 4^N experimental configurations for full quantum process tomography, and in particular only one experimental setting for estimating certain parameters (e.g. relaxation times) [7, 8]. Experimental efforts in this direction include a partial and non-scalable implementation of DCQD [9, 10], an ancilla-assisted process tomography [4, 5] and a joint effort efficiently implementing DCQD in a photonic system [11].

Alternatively, efficient gate-fidelity estimation methods such as randomized benchmarking [12], or tomographic methods such as selective and efficient QPT [13, 14] and compressed sensing for quantum process tomography [15–17] have recently been developed to overcome the exponential increase of the required experimental configurations. Generally, these methods are tailored to estimate a polynomial number of effective parameters, such as gate fidelity [12] or when we can make a sparse quantum process/Hamiltonian assumption from a priori knowledge about the quantum system [17]. For example, the estimation of the dynamical parameters T_1 and T_2 (longitudinal and transverse relaxation times [1]) is a task involving two non-commuting observables (e.g. σ_x and σ_z) that cannot be measured simultaneously. These parameters describe the influence of noise on atomic-, molecular- and spin-based systems induced by the interaction with the environment. An alternative approach based on DCQD, henceforth called Direct Characterization of Relaxation Times (DCRT), enables the measurement of both T_1 and T_2 *simultaneously* with a single experimental configuration [18].

In this work, we apply the DCQD technique and extensions on a system of trapped $^{40}Ca^{+}$ ions. Single-qubit processes are reconstructed with four experimental configurations using DCQD, and alternatively with just a single configuration using a generalized measurement (GM). In addition, we quantify the relaxation times T_1 and T_2 in our system with a single configuration. This technique can also characterize more realistic environments affecting not only the probe but also the ancilla qubit collectively.

In the following, we consider quantum processes which can be described by a completely positive, convex-linear and trace-preserving map E mapping the input state ρ onto the output state ρ'. For a single qubit this can be written as

$$E : \rho \to \rho' = \sum_{m,n=1}^{4} \chi_{m,n}\ \sigma_m\ \rho\ \sigma_n^{\dagger}, \qquad (1)$$

with σ_m, σ_n the Pauli operators $\{\mathbb{1}, \sigma_x, \sigma_y, \sigma_z\}$ and χ a semi-positive matrix containing complete information about the process. In standard quantum process tomography (SQPT) the process is applied to four input states

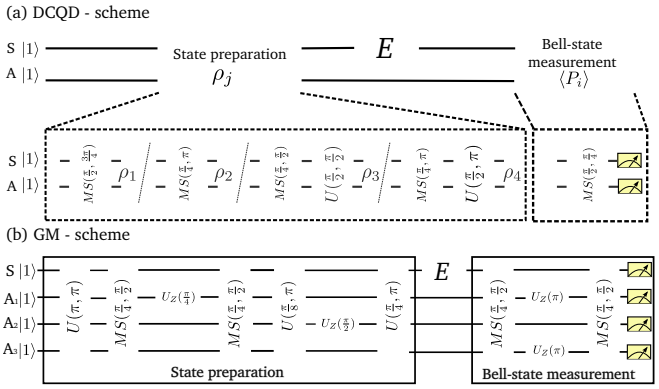

FIG. 1. (color online) Procedure to characterize a single-qubit process with DCQD and a GM. In DCQD (a) each experimental configuration consists of the preparation of one of four input states ρ_j entangled between the system ion S and the ancilla ion A. The process E is applied on S followed by a BSM on the output state $E(\rho_j)$, which consists of a single MS operation followed by a projection onto the computational basis. (b) Generalized measurement via many body interactions (see text).

and followed by full state tomography of each output state, which for a trace preserving map consists of three measurements, resulting in $4 \times 3 = 12$ experimental configurations. In DCQD these four input states are replaced by four entangled states between the system qubit S and an ancilla qubit A, and the state tomography is replaced by a single Bell-state measurement (BSM), as shown in Fig. 1(a), with a total of $4 \times 1 = 4$ experimental configurations (Bell states $|\Psi^{\pm}\rangle$ and $|\Phi^{\pm}\rangle$ as defined in Table I). The probabilities $p_{i,j}$ of measuring the Bell-state projector P_i for each input state ρ_j shown in Table I are determined, according to Refs. [7, 19], by

$$p_{i,j} = \mathrm{Tr}(P_i\ E(\rho_j)) = \sum_{m,n=1}^{4} \chi_{m,n}\ \Lambda_{m,n}^{i,j} \qquad (2)$$

$$\Lambda_{m,n}^{i,j} = \mathrm{Tr}(P_i(\sigma_m \otimes \mathbb{1})\rho_j(\sigma_n \otimes \mathbb{1})^{\dagger}).$$

Therefore the process matrix χ can be calculated directly by linear inversion of the matrix Λ. The set of input states ρ_j and the Bell-state projectors P_i have to be determined such that the 16 equations in Eq. (2) are linearly independent, which ensures that Λ is invertible (Table I).

Our experiments were realized on a system consisting of $^{40}Ca^{+}$ ions confined to a string in a linear Paul trap [20]. Each ion represents a logical qubit which is encoded in the electronic levels $D_{5/2}(m = -1/2) = |0\rangle$ and $S_{1/2}(m = -1/2) = |1\rangle$. Each experimental cycle consists of an initialization of the ions in their internal electronic and motional ground states followed by a coherent manipulation of the qubits and finally a detection of the quantum state. State initialization is realized by optical pumping into the $S_{1/2}(m = -1/2)$ state after cooling the axial centre-of-mass mode to the motional ground state.

Input states $\rho_j = \lvert\psi_j\rangle\langle\psi_j\rvert$	Bell-state basis
$\lvert\psi_1\rangle = \lvert 00\rangle + \lvert 11\rangle$	$\lvert\Phi^{+}\rangle = \lvert 00\rangle + \lvert 11\rangle$
$\lvert\psi_2\rangle = \alpha\lvert 00\rangle + \beta\lvert 11\rangle$	$\lvert\Psi^{+}\rangle = \lvert 01\rangle + i\lvert 10\rangle$
$\lvert\psi_3\rangle = \alpha\lvert++\rangle_x - \beta\lvert--\rangle_x$	$\lvert\Psi^{-}\rangle = \lvert 01\rangle - i\lvert 10\rangle$
$\lvert\psi_4\rangle = \alpha\lvert++\rangle_y - \beta\lvert--\rangle_y$	$\lvert\Phi^{-}\rangle = \lvert 00\rangle - \lvert 11\rangle$

TABLE I. Input states and BSM basis used for the implementation of DCQD ($|\pm\rangle_x = \frac{|0\rangle \pm |1\rangle}{\sqrt{2}}$, $|\pm\rangle_y = \frac{|0\rangle \pm i|1\rangle}{\sqrt{2}}$). The determinant of Λ in Eq. (2) is maximized for $\alpha = \cos(\frac{3\pi}{8}$ and $\beta = \exp(i\frac{\pi}{2})\sin(\frac{3\pi}{8}))$ to ensure the invertibility [19]. The BSM is realized by a measurement with the projectors $P_i = \{|\Phi^{\pm}\rangle\langle\Phi^{\pm}|, |\Psi^{\pm}\rangle\langle\Psi^{\pm}|\}$.

The manipulation of the qubits is implemented by coherently exciting the $S_{1/2} \leftrightarrow D_{5/2}$ quadrupole transition with laser pulses. Finally, the population of the qubit states is measured by exciting the $S_{1/2} \leftrightarrow P_{1/2}$ transition and detecting the fluorescence light, using electron shelving [21]. Our setup is capable of realizing collective qubit rotations $U(\theta, \phi) = \exp(-i\frac{\theta}{2}\sum_i[\sin(\phi)\sigma_y^{(i)} + \cos(\phi)\sigma_x^{(i)}])$ via a laser beam addressing the entire register as well as Mølmer-Sørenson entangling gates $MS(\theta, \phi) = \exp(-i\frac{\theta}{4}[\sum_i \sin(\phi)\sigma_y^{(i)} + \cos(\phi)\sigma_x^{(i)}]^2)$ [22, 23]. Additionally we are able to perform single-qubit rotations on the i-th ion of the form $U_Z^{(i)}(\theta) = \exp(-i\frac{\theta}{2}\sigma_z^{(i)})$ by an off-resonant laser beam, which addresses individual ions. The input states for DCQD of Table I are prepared by applying collective entangling operations and qubit rotations as shown in Fig. 1(a). For example, the input state ρ_2 is created by the non-maximally entangling operation $MS(\frac{\pi}{4}, \pi)$. Our two-qubit entangling operation generates Bell states with a fidelity of $\approx 99\%$ in 120 μs. The BSM is experimentally realized by a maximally entangling operation $MS(\frac{\pi}{2}, \frac{\pi}{4})$, which maps from the Bell-state basis to the computational basis $\{|00\rangle, |01\rangle, |10\rangle, |11\rangle\}$, followed by individual-ion-resolving fluorescence detection with a CCD camera.

As an example of the reconstruction method, consider the first input state $\rho_1 = |\Phi^{+}\rangle\langle\Phi^{+}|$. If the process E is the identity $\mathbb{1}$, the expectation value of the BSM-projector P_1 is 1 which is equivalent to detecting both ions in the state $|11\rangle$ after the BSM. If a bit flip occurs on the system ion, the output state is then mapped onto the state $|01\rangle$ by the BSM ($\langle P_2\rangle = 1$). The considerations are similar for a phase-flip, or bit- and phase-flip processes. Therefore, the diagonal elements $\chi_{m,m}$ of the superoperator χ corresponding to $\mathbb{1}$, σ_x, σ_y, and σ_z are detected by a single input state in combination with one BSM.

We demonstrate the DCQD method by characterizing the full quantum process of implemented unitary rotations σ_x and σ_y as well as non-unitary processes such as amplitude- and phase-damping [24]. The χ matrices reconstructed from the measured probabilities, are

shown in Fig. 2(a,b) for σ_x and σ_y rotations. A single-qubit process can also be visualized by transforming the pure states lying on a Bloch sphere. In this Bloch sphere representation, decohering processes map the unit Bloch sphere (shown as a transparent mesh) to an ellipsoid of smaller volume [1]. Implemented amplitude- and phase-damping processes taking place with a 60% probability are shown in this representation in Fig. 2(d,f) [24]. For each input state the experiment was repeated up to 250 times for statistical averaging. All processes were reconstructed with a maximum likelihood algorithm to ensure trace preservation and positivity of the superoperator χ [25]. The fidelity F of a process describes the overlap between the measured χ_{meas} and the ideal superoperator χ_{id}. For each process we calculate the overlap between χ_{meas} and χ_{id} using the entanglement fidelity extended to be applicable also for non-unitary processes [25–27]. Table II shows the calculated fidelities for the implemented DCQD and for SQPT. The uncertainty in the fidelity was estimated by parametric bootstrapping based on projection noise in our measurement [28].

Target process	DCQD, F (%)	SQPT, F (%)
$\mathbb{1}$	97.5 ± 0.6	98.1 ± 1.3
σ_x	96.5 ± 1.0	98.1 ± 1.3
σ_y	96.6 ± 1.4	97.5 ± 1.4
amplitude damping	95.3 ± 1.9	95.2 ± 2.7
phase damping	97.4 ± 0.8	95.7 ± 0.8

TABLE II. Calculated process fidelities F between implemented and target processes as characterized with DCQD and SQPT. All processes were measured with a total of 1000 experimental cycles, which correspond to 1000/4 cycles per experimental configuration for DCQD and 1000/(4×3)∼84 for SQPT. The SQPT of the phase damping process was measured with a total of 3000 experimental cycles.

Full QPT of a single-qubit process is also possible with a single experimental configuration by using additional ancillas and a generalized measurement (GM). Here, we expand the dimension of the Hilbert space $H_A \otimes H_S$, with the system Hilbert space H_S and the ancilla Hilbert space H_A, such that the dimension of the total Hilbert space is equal to the number of free parameters in the process matrix χ [6]. For a single-qubit process one has to determine all 16 superoperator elements $\chi_{m,n}$ which leads to an 8 dimensional ancilla Hilbert space. Therefore we used three ancilla qubits A_1, A_2 and A_3 to quantify a full process E acting on the system qubit S. This GM is realized by entangling the system and ancilla qubits using many-body interactions [22, 23], then applying the process E on S and finally performing BSMs on two pairs. Figure 1(b) shows the sequence implemented for this GM which proceeds as follows. First, we create an entangled input state using maximally and non-maximally entangling Mølmer - Sørenson interactions in combination with global and addressed single-qubit rotations. After applying the process E on S we perform a pairwise BSM on the combined output state by implementing two non-maximally entangling operations $MS(\frac{\pi}{4})$ and two addressed AC-Stark pulses $U_Z^{(1)}(\pi)$ and $U_Z^{(3)}(\pi)$, which separate the entangled system $H(S, A_1, A_2, A_3)$ into a product state of two subsystems $H(A_1, A_3) \otimes H(S, A_2)$. These operations are equivalent to two pairwise maximally entangling gates $MS(\frac{\pi}{2})$ acting on the two subsystems $H(A_1, A_3)$ and $H(S, A_2)$. The 16 results of the measurement are directly linked to the 16 superoperator elements $\chi_{m,n}$ by a matrix Λ similar to Eq. (2). Using this technique we reconstructed unitary processes $\{\mathbb{1}, \sigma_x = U(\pi, 0), \sigma_y = U(\pi, \frac{\pi}{2}), \sigma_z = U_z^{(1)}(\pi)\}$ acting on a single qubit with a fidelity of $\{99.70 \pm 0.02, 97.30 \pm 0.29, 99.80 \pm 0.01, 99.40 \pm 0.02\}$%. All processes were measured with a total of 5000 cycles.

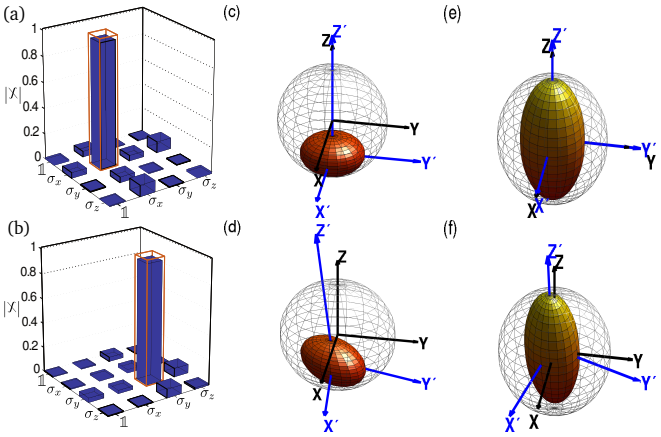

FIG. 2. (color online) Experimental results of DCQD for unitary and decoherence processes. (a-b) Results of the measured superoperator χ for the rotation operations $U(\pi, 0)$ in (a) and $U(\pi, \pi/2)$ in (b). Ideally, the target processes have only nonzero elements at positions indicated by the orange-bordered bars. (c-d) Bloch sphere representation of the ideal (c) and measured (d) amplitude damping process with 60% probability [22]. (e-f) Bloch sphere representation of the ideal (e) and measured (f) phase damping process with 60% probability [22]. Bloch sphere axes in black evolve into the spheroid primed axes in blue. A slight imperfection due to residual light on the ancilla ion can be observed as a rotation of the spheroids in the measured decohering processes.

In contrast to previous QPT measurements of engineered processes, the process of phase (amplitude) damping occurs naturally in our system due to magnetic field fluctuations (spontaneous decay) [29]. The dynamical parameters T_1 and T_2 can, however, be determined simultaneously with only the first input state ρ_1 being subject to the DCQD scheme even if the damping processes act collectively on both qubits (as in our experimental system [29]). This method, named DCRT above, consists of preparing an input Bell state $\rho_1 = |\Phi^+\rangle\langle\Phi^+|$, exposing both qubits to the damping processes for a time t and a final BSM, which yields the diagonal elements $\chi_{i,i}$ of the

process matrix. As described in the supplementary material [24] and assuming Markovian noise the dynamical parameters are then given by

$$\begin{aligned} e^{-\frac{N^2 t}{T_2}} &= \chi_{1,1} - \chi_{4,4} \\ &= \mathrm{Tr}\left\{\left[|\Phi^+\rangle\langle\Phi^+| - |\Phi^-\rangle\langle\Phi^-|\right] \mathrm{E}\left(|\Phi^+\rangle\langle\Phi^+|\right)\right\}, \end{aligned} \tag{3}$$

$$1 + 2e^{-\frac{2t}{T_1}} - 2e^{-\frac{t}{T_1}} = 1 - 2(\chi_{2,2} + \chi_{3,3}), \tag{4}$$

with N the number of ions. From the entries of the χ matrix corresponding to $\mathbb{1}$ and σ_z (σ_x and σ_y) operations, T_2 (T_1) depends on the probability that no error or phase flips (bit flips) occur on the entire system. A fit of DCRT measurements $\chi_{i,i}$ to Eqns. (3-4) at different times t thus yields T_1 and T_2 using a single experimental configuration. We explored this DCRT technique in our experimental system. The measurement results of the decoherence estimation are shown in Fig. 3(a). The green dots show the difference between the diagonal elements $\chi_{1,1}$ and $\chi_{4,4}$ as a function of the waiting time t. The spontaneous decay of the system is shown in Fig. 3(b) by plotting $1 - 2(\chi_{2,2} + \chi_{3,3})$ as a function of time. For every waiting time t the experiment was repeated up to 250 times to gain significant statistics.

We can compare the DCRT technique with two traditional methods that use product input states: Ramsey-contrast measurements for phase-decoherence estimation and direct spontaneous-decay measurements [30]. A Ramsey-contrast measurement is realized by initializing the ion in the state $(|0\rangle + |1\rangle)/\sqrt{2}$ by a global rotation $U(\frac{\pi}{2}, 0)$, followed by a waiting time t and finally applying a second rotation $U(\frac{\pi}{2}, \phi)$ in which the phase ϕ is varied. The observed contrast as a function of ϕ corresponds to the preserved phase coherence. Spontaneous-decay measurements, instead, consist of measuring the probability of detecting both ions in the excited state $|0\rangle$ as a function of time. The results of these Ramsey-contrast (spontaneous-decay) measurements are shown in Fig. 3(a) (Fig. 3(b)) as red diamonds (blue triangles). The measured relaxation times corresponding to the traditional methods are called T_1^{trad} and T_2^{trad}. The exponential fit (green line) of Eq. (3) to the data was estimated with $N = 2$ (collective dephasing) and yields T_2^{DCRT}=18.8(5) ms. The Ramsey-contrast measurements (red diamonds) were carried out on a single ion and yield a coherence time of T_2^{trad}=19.4(8) ms. The green dotted line in Fig. 3(a) corresponds to the fitted function to Eq. (3) (green line) with $N = 1$ instead of $N = 2$ and shows good agreement with the single-ion Ramsey-contrast measurement. Therefore the DCRT technique enables the characterization of the phase decoherence of the collective system (green line) and also gives a conclusion about the phase decoherence of a single ion (green dotted line). An exponential fit of the decay data of Fig. 3(b) to Eq. (4) gives the characteristic lifetime $T_1^{DCRT} = 1130(47)$ ms for the DCRT technique (green line) and $T_1^{trad} = 1160(30)$ ms for the traditional method (blue dotted line), which are in good agreement with previously measured values [31] of 1148(18) ms.

In summary, we have experimentally demonstrated two different approaches for the full characterization of single-qubit quantum processes, lowering the required experimental configurations from 12 to 4 using DCQD and a single configuration via the GM method. The reconstruction of coherent and incoherent processes was shown with fidelities of $\geq 97\%$ using DCQD. In particular, we have observed a lower statistical uncertainty of the fidelity of some of the processes compared to the SQPT. Nevertheless, a matter of further investigations is a comparison of the scaling in the number of experimental cycles required for the SQPT and DCQD to achieve a target uncertainty in the fidelity (e.g. see identity process in Table II). Experimentally, a reduced number of experimental configurations implies a substantial reduction of measurement time for a full QPT using DCQD as compared with SQPT (e.g., from 35 days to 1 day, see [24]). In addition, the DCRT technique, based on the DCQD protocol, was used as a powerful tool to characterize the noise in our system by measuring the relaxation times T_1 and T_2 simultaneously with one experimental setting. This technique indicates good agreement with traditional methods as Ramsey-contrast and spontaneous decay measurement. In principle, there is an improvement of a factor of two in the measurement time if T_1 is of the same order of magnitude as T_2, which is not the case for our setup. In contrast, spin-based solid state systems are collectively affected by noise and $T_1 \approx T_2$, which would lead to a significant improvement of the measurement time [32]. Another application of DCRT could be for biological systems where dissipative dynamics play a crucial role [33, 34]. The same measurement procedure can also be used as a tool to quantify Hamiltonian parameters efficiently, which can not be realized with other currently known techniques besides full QPT [8, 18]. Furthermore, DCQD offers the capability to reveal the non-Markovian properties of system-bath interactions [8, 35].

We gratefully acknowledge support by the Austrian Science Fund (FWF), through the Foundations and Applications of Quantum Science (SFB FoQus), by the European Commission AQUTE, by IARPA, QuISM MURI and DARPA QuBE Program as well as the Institut für Quantenoptik und Quanteninformation GmbH. Julio T. Barreiro acknowledges support by a Marie Curie International Incoming Fellowship within the *7th* European Community Framework Programme.

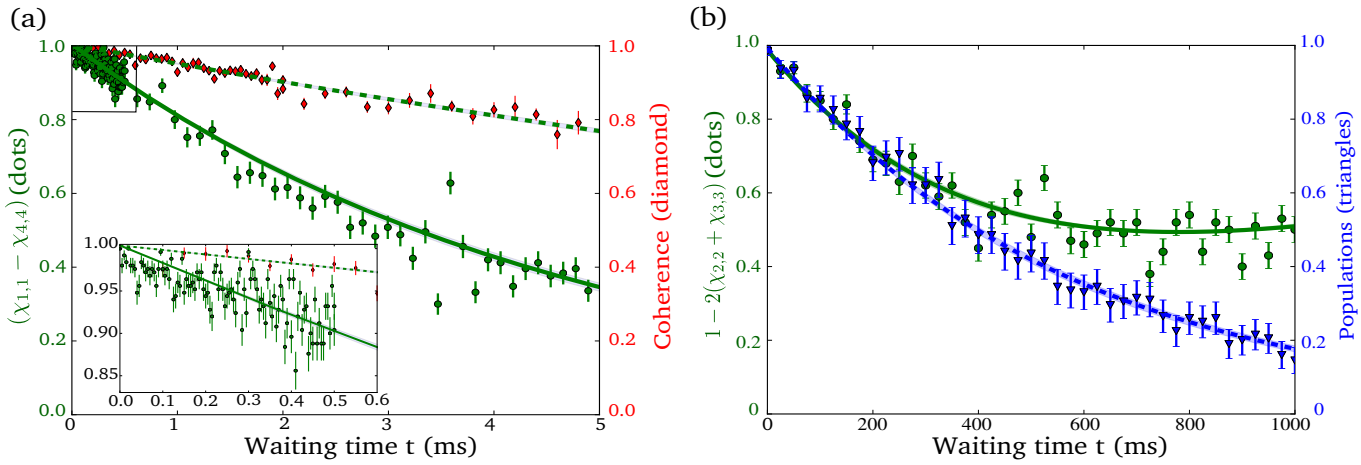

FIG. 3. (color online) Simultaneous measurement of phase decoherence (a) and the spontaneous decay (b) of a two-qubit system. The DCRT technique (green dots) is compared to a Ramsey-contrast measurement (red diamonds) and a spontaneous-decay measurement (blue triangles) (see text). The measurement using the DCRT method in (a) was carried out on the entangled two-qubit system ($\exp(-\frac{4t}{T_2^{DCRT}})$ scaling) whereas the red diamonds were measured on a single qubit with the Ramsey-contrast technique ($\exp(-\frac{t}{T_2^{trad}})$ scaling). The shaded areas correspond to the envelope of the curves with the decay times $T_{1,2}^{DCRT,trad}\pm\Delta T_{1,2}^{DCRT,trad}$, considering the statistical errors $\Delta T_{1,2}^{DCRT,trad}$. The relaxation time measurements, using the DCRT method and, in comparison, the traditional Ramsey-contrast and spontaneous decay measurement, yield: T_2^{DCRT}=18.8(5) ms, T_2^{trad}=19.4(8) ms, T_1^{DCRT} = 1130(47) ms and T_1^{trad} = 1160(30) ms.

* Present address: Ludwig-Maximillians-Universität and Max-Planck Institute of Quantum Optics; Julio.Barreiro@gmail.com
† mohseni@mit.edu

[1] M. A. Nielsen and I. L. Chuang, *Quantum Compuation and Quantum Information* (Cambridge University Press, 2009).
[2] A. M. Childs, I. L. Chuang, and D. W. Leung, Phys. Rev. A **64**, 012314 (2001).
[3] Changing experimental configurations is an overhead to be considered in several quantum architectures such as photons and ions.
[4] G. M. D. Ariano and P. L. Presti, Phys. Rev. Lett. **86**, 4195 (2001).
[5] J. B. Altepeter et al., Phys. Rev. Lett. **90**, 193601 (2003).
[6] M. Mosheni, A. T. Rezakhani, and D. A. Lidar, Phys. Rev. A **77**, 032322 (2008).
[7] M. Mohseni and D. A. Lidar, Phys. Rev. Lett. **97**, 170501 (2006).
[8] M. Mohseni and A. T. Rezakhani, Phys. Rev. A **80**, 4 (2009).
[9] Z. W. Wang et al., Phys. Rev. A **75**, 044304 (2007).
[10] W. T. Liu et al., Phys. Rev. A **77**, 032328 (2008).
[11] T. Graham et al., arXiv **1205.2587**, 4 (2012).
[12] E. Knill et al., Phys. Rev. A **77**, 012307 (2008).
[13] C. Schmiegelow et al., Phys. Rev. Lett. **104**, 123601 (2010).
[14] A. Bendersky, F. Pastaeski, and J. P. Paz, Phys. Rev. Lett. **100**, 190403 (2008).
[15] A. Shabani et al., Phys. Rev. A **84**, 1 (2011).
[16] A. Shabani et al., Phys. Rev. Lett. **106**, 1 (2011).
[17] D. Gross et al., Phys. Rev. Lett. **105**, 250401 (2010).
[18] M. Mohseni, A. T. Rezakhani, and A. Aspuru-Guzik, Phys. Rev. A **77**, 042320 (2008).
[19] M. Mohseni et al., Phys. Rev. A **81**, 032102 (2010).
[20] F. Schmidt-Kaler et al., Appl. Phys. B **77**, 789 (2003).
[21] W. Nagourney, J. Sandberg, and H. Dehmelt, Phys. Rev. Lett. **56**, 2797 (1986).
[22] A. Sørenson and K. Mølmer, Phys. Rev. A **82**, 1971 (2000).
[23] G. Kirchmair et al., New J. Phys. **11**, 023002 (2009).
[24] See supplemental material.
[25] Z. Hradil, J. Rehacek, J. Fiurasek, and M. Jezek, *Quantum State Estimation* (Springer, 2004).
[26] P. E. M. F. Mendonca et al., Phys. Rev. A **78**, 11 (2008).
[27] M. A. Nielsen, Phys. Lett. A **303**, 249 (2002).
[28] B. Efron and R. Tibshirani, "Statistical science," (Institute of Mathematical Statistics, 1986) pp. 54–57.
[29] T. Monz et al., Phys. Rev. Lett. **106**, 130506 (2011).
[30] F. Schmidt-Kaler et al., J. Phys. B: At. Mol. Opt. Phys. **36**, 623 (2003).
[31] P. Staanum et al., Phys. Rev. A **69**, 032503 (2004).
[32] X. Hu, R. de Sousa, and S. D. Sarma, *Foundations of Quantum Mechanics in the Light of new Technology* (eProceedings, 2001).
[33] M. Mohseni et al., J. Chem. Phys. **129**, 174106 (2008).
[34] J. Yuen-Zhou et al., PNAS **108**, 17615 (2011).
[35] J. T. Barreiro, Nature Physics **7**, 927 (2011).